The role of theta oscillations in the spatial functions of the hippocampal formation

Manos Protonotarios

Supervisors: John O'Keefe & Neil Burgess

CoMPLEX

Essay Two,

March 16, 2011

Word Count[1]: 4596

[1] without figures, tables, displayed equations, references, acknowledgments and appendices

Page intentionally left blank

Contents

Page intentionally left blank

1 Abstract

In this essay a temporal analysis of the electroencephalogram (EEG) and the firing data of identified grid cells of previously conducted experiments with freely moving rats is presented. The study is focused mainly on the subset of data that coincide with low speed time intervals (v<5cm/s or v<10cm/s) and it is done in the framework of recently presented theories [1][2][3] describing the grid cell firing characteristics on the basis of an oscillatory interference model.

2 Introduction

The role of the hippocampal formation on the spatial cognition and representation is being researched intensively for more than three decades. Recent advancements in neuroscience related to the functioning and the properties of place cells, discovered in the rat hippocampus, have enriched our intuition about how the spatial representation but also the self-perception in space might be implemented on the neuronal level. Place cells and grid cells, discovered later in the entorhinal cortex, because of their unique spatial correlation properties initiated a quantum leap forward in the development of quantitative theories and models about the temporal encoding of spatial information. They also suggested ideas of how path integration could be possible contributing to self-navigation understanding.

The oscillation interference theory which explains the complex and highly organized grid field pattern and some aspects of the place cell properties based on elegant and simple principles provides at the same time specific and testable predictions e.g. the increase of both the EEG theta frequency and the intrinsic firing frequency of the grid cells with the increasing speed of the freely moving tested animal (rat).[1][2][3] Analysis of these data in the case of speeds greater than 5cm/s had already been conducted and in this essay we are focusing mostly on speeds lower than 5cm/s.

In the following section some basic background knowledge is presented in relation to the hippocampal formation anatomy and interconnections, since place cells and grid cells are located there. A reference to theta oscillations, place cells and grid cells follows. A brief reference to the main idea behind the theory of the oscillation interference is made later on and the data analysis method and the discussion of the analysis follow. The essay ends with the Conclusions section. [4]

3 Biological Background

3.1 Hippocampal Formation

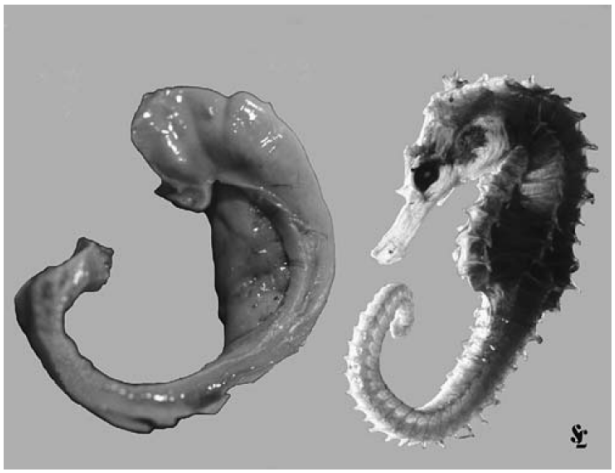

Figure 3-1. Dissected human hippocampus (left) compared to Hippocampus leria (right). (From [5], source: Courtesy of Professor Laszlo Seress, University of Pecs.)

The hippocampus' role in the spatial representation is essential. In addition, many general principles of neuroscience were discovered from the hippocampus studies, e.g. the role of oscillations in neuronal networks, identification of the synapses type, transmitters and receptors [6]. Its single cell laminar neuroanatomic structure, the clearly organized interconnection circuits, its high plasticity and its substantial role in memory and spatial cognition are only some of the features that justify the vivid research being conducted during the last decades. Although the human hippocampus is about 100 times larger than that of the rat, the main architecture is very common implying common functional properties and possible applications of rat experimental results to humans [7].

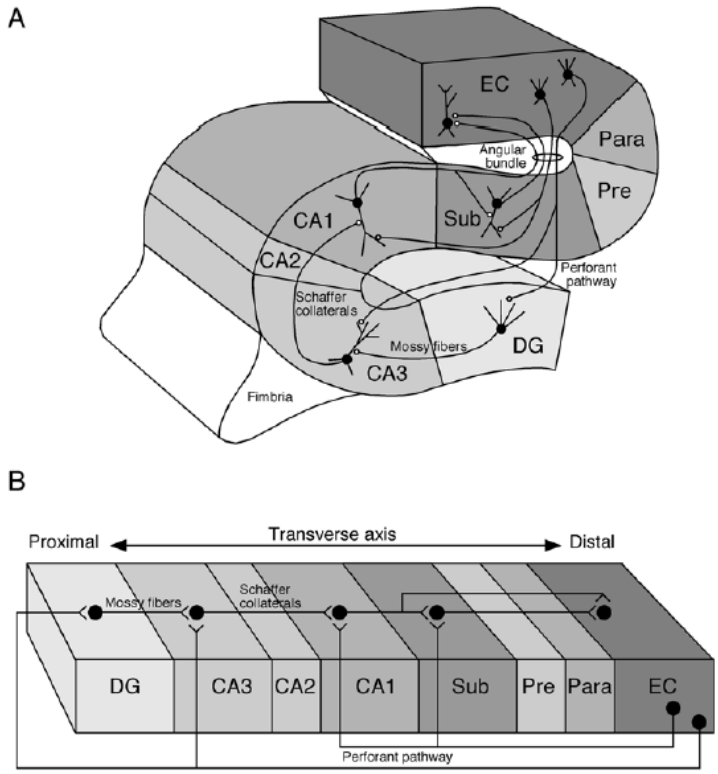

Figure 3-2. The hippocampal formation – Subdivisions and neuronal connections. A.Dentate Gyrus (DG), CA3, CA2, CA1 fields, Subiculum (Sub), Presubiculum (Pre), Parasubiculum (Para) and Entorhinal Cortex (EC). B. Transverse axis of the hippocampal formation. (From [7])

The hippocampal formation is a functional system of related brain regions containing the hippocampus, the dentate gyrus, the subiculum, the presubiculum, the parasubiculum and the entorhinal cortex (Figure 3-2) [6]. In the rat it has an elongated slightly curved shape extending from the middle of the brain over and behind the thalamus. The hippocampus is divided into three subfields, namely CA3, CA2 and CA1 (CA: from cornu ammonis, Latin for horn of the ram – terminology by Lorente de No) and the Entorhinal Cortex is divided into six layers (layers I to VI). The connections in the hippocampal formation are not reciprocal as those between regions of the neocortex. Since, input from the neocortex reaches the hippocampal formation through the entorhinal cortex and furthermore the main path from there to the dentate gyrus (perforant path) is unidirectional, the entorhinal cortex is a convenient starting point for following the entire circuit of connections. Neurons from layer II of the EC project to the CA3 and the DG through the aforementioned perforant pathway while neurons from layer III of the EC project to the CA1 through both the perforant and another complex fiber system pathway, called alvear. The information received by the CA2, CA3 cells from the EC is probably similar. However, cells in CA1

receive different input from the EC, depending on their relative position in the field [7]. Input originating from the medial entorhinal cortex (MEC) reaches the proximal portion of the CA1 whereas input originating from the lateral EC reaches the distal portion of the CA1. Among the hippocampal cells only those located in the CA1 exhibit projections to the EC and these fibers terminate to approximately the same region inside the EC where their inputs originated. The hippocampus fields are all similar in terms of their layer structure having a principal cellular layer called pyramidal which is more tightly packed in the case of CA1. Pyramidal cells of CA3 and CA2 present a distribution of dendritic length with the largest ones located distally (16-18mm total dendritic length) and the smallest ones located near the DG (8-10mm total dendritic length) receiving less direct input from the EC. On the other hand, the pyramidal cells of the CA1, regardless of their position, have very similar length and dendritic structure.[7]

The EC contains in layer II small clustered pyramidal cells and stellate cells of medium to large size while in layer III it contains mostly pyramidal cells. EC apart from providing the main input pathway of information from neocortex to the hippocampus, is also the main output of the processed information back to the neocortex.[7]

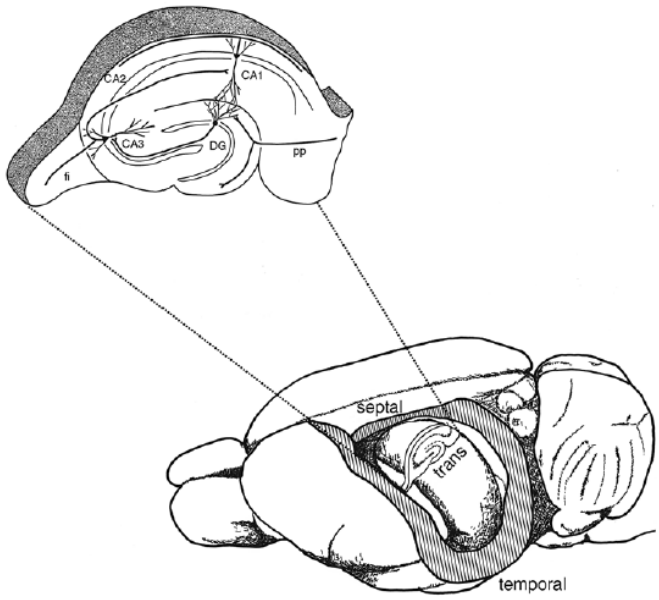

Figure 3-3. Drawing showing the septotemporal and transverse axes of the hippocampal formation of the rat. (From [7])

3.2 Theta Oscillations

In 1969 Vanderwolf [8] implanted electrodes at the dorsal hippocampal formation and other brain structures of rats and recorded the electrical activity of the neurons (electroencephalogram or EEG), while the animals were able to move freely inside a box, in an attempt to correlate the recordings with different observed behaviors. In the case of the hippocampus he distinguished three patterns of electrical activity: Regular activity named Rhythmical Slow Activity or theta, related to voluntary

movements (such as walking, jumping etc) or arousal/attention and two other types of irregular activity related to automatic behavior (licking, chewing etc) and other behavioral states. Until now four rhythmical patterns have been identified in the hippocampus of the rat, with theta being one of them. The frequency range of the, often sinusoidal, theta waves is 6-12Hz. Of the two types of theta oscillations, the one (t-theta) was found to be correlated with transitional movements of the rat in space. Furthermore, the frequency was shown to increase with the increase of speed [9]. Theta amplitude though, does not seem to correlate with speed in rats.

Since the EEG reflects the collective activity of a large number of neurons, the theta oscillation implies a cell synchronicity. Indeed, theta activity in different hippocampal locations has been recorded and a systematic temporal relation of even relatively far located neurons modulated by the theta waves was verified. Therefore, it is possible that theta wave organizes the hippocampal formation in a temporal mode synchronizing the activity of different subdivisions. An additional possible role of theta waves is to provide a temporal periodic reference signal for the spiking of the hippocampal neurons. [10]

3.3 Place cells

The question of space representation in the brain of humans and animals has been placed in a radically productive framework after the discovery by O' Keefe and Dostrovsky [11] of cells in the hippocampus of rats with firing activity related to spatial parameters. They recorded, in particular, with the use of lightweight microdrives placed on the rat's head, increased firing activity of certain cells in the dorsal hippocampus and dentate gyrus when a controlled tactile stimulus was combined with the rat being situated in a particular position and facing in a particular direction. After isolating other possible factors as the cause for the increased firing (olfactory and tactile cues or sound stimuli that could affect the orientation preference etc), it was suggested that these cells could play the role of a spatial reference map, linked also to the spatial environment learning process. Further studies confirmed pyramidal cells (place cells) of the hippocampus that fired only when the rat was in a certain location in a familiar environment (place field of the cell) [12]. The entire spatial environment can be represented by different place cells throughout the hippocampus with no topographical relation between the two. The same cell can represent a different place field in another environment and all place cells together constitute a dynamic representation of the space and the position of the animal in that space. It is however, very probable that a place cell does not have a place field in every setting. The properties of the place fields such as the shape and the size depend on the characteristics of the enclosure and on the location of the cell. A small percentage of them relate to edge fields, i.e. they are active near the edge of the environment. When the rat enters a new environment stable place cells are built relatively quickly and they are controlled by distal visual cues.

Place field can be depicted by splitting the available space in a set of small squares and attributing a colour to each square depending on the ratio of the number of spikes recorded for that square divided by the amount of time the animal occupied in this square and scaled to the place cell's peak rate (map plot). [4][10]

Place fields in open-field environments are non-directional, in the sense that their firing does not depend on the direction of the animal's head, while in restricted linear tracks they are. Even the same cell can exhibit both kinds of behavior depending on the constraints. [13][10]

Place cells fire in bursts when the rat is in the cell's field at a time spacing which corresponds to the theta frequency. Experiments in narrow tracks [13] showed that the phase of the bursts of CA1 place cells advances earlier in relation to the theta wave during the passage of the rat through the field. This effect, called phase precession, was verified in 2-dimensional environments as well [14]. [10][4][15]

3.4 Grid Cells

The persistence of place signals in the CA1, even after the removal of the dentate gyrus inputs to the hippocampus, rejected the hypothesis that these signals originated in the hippocampal network and the perforant-path projections of the layer III of the EC became a possible input path. Projection neurons of layers II and III of the medial EC (MEC) studied afterwards revealed a place-cell-like firing pattern with fields not restricted in a limited area as in place cells but extending in a form of a periodic triangular array (grid) and covering the whole available environment (Figure 3-4) [16][17]. The geometric characteristics of such a grid are the grid spacing, the orientation relative to a fixed axis and its displacement relative to a reference point. Grid cells in deeper EC exhibit firing which is also modulated by the head-direction. The grid spacing of closely located grid cells is the same but it increases as we move away from the dorsal boundary of the EC. However, the totality of the grid cells of an animal shares the same orientation. The phase precession effect observed in hippocampal place cells is also present in the EC layer II stellate cells. [18][19][17][20][2][21][22][4]

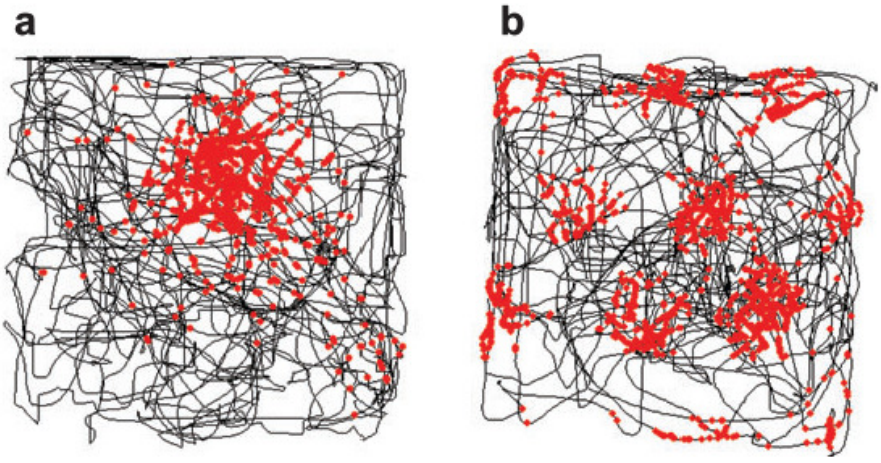

Figure 3-4. (a) Place cell field from the hippocampus cell and (b) grid cell field from the MEC cell. The red spots represent the position of the rat at the moment of the firing of the cell and the black curved line the rat's trajectory. The place cell field covers a specific limited location of the environment while the grid cell field is extended in a tessellated manner to the entire available environment. (From [4])

4 The Model of Grid Cell Pattern Formation

Most theories attempting to explain the formation of grid cell pattern suppose that there is an integrating mechanism of speed and direction based on the MEC cells aided by sensory cues to set up the initial parameters or correct cumulative error. Some models [23] suppose that the mechanism is based on local network activity while others are concentrated on a single cell level [1][13]. O'Keefe and Recce [13] proposed a model, on a single cell level, for the aforementioned phase precession and the formation of the place fields for the 1-dimension case based on the interference of two oscillations of frequencies close to theta. Assuming that one oscillation represents data projected to the cell in a slightly faster frequency than theta (by an amount proportional to the speed) and the other frequency originates from the EEG at theta, the resulting oscillation has a slow envelope which determines the place field while the fast beat oscillation determines the firing rate. The shape of the envelope is in accordance with the bell-shaped place fields and the progressive move of the wave packet to earlier phases is in accordance with the observed phase precession of the firing. The phase information provides a high resolution measure of location and the linear dependence of the faster frequency on the speed keeps the size of the field constant and independent of changes in the speed. Additionally, variations in firing rate seem to be of less importance in this kind of phase representation for the location.[2][4]

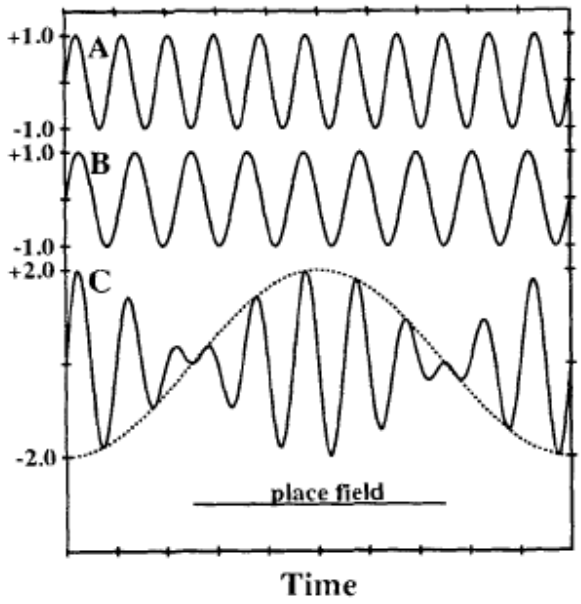

Figure 4-1. Model of the interference pattern for the place field formation in one dimension: Two similar sinusoidal oscillations (A, B) differing slightly in the frequency create an interference pattern which determines the place cell firing (C). (From [13])

There are two types of interacting oscillatory inputs; one termed as *somatic intrinsic oscillator* with frequency which is close to the theta frequency (or baseline frequency $f_b(t)$) originating from the medial septal pacemaker and the other termed as *dendritic oscillator* (active membrane potential

oscillation MPO) with an increased frequency relative to the somatic frequency which depends on the synaptic input. These signals are summed linearly at the cell membrane potential. The MPO's frequency f_a depends proportionally on the speed so that $f_a(t) - f_b(t) = \beta s(t)$, where s is the speed and β a constant. By integrating this equation it is obvious that the difference in phase between the oscillation and the theta wave will be proportional to the distance travelled in the field.

Burgess et al. [2][3] extended the previous interference model to 2-dimensional environments by assuming more than one Velocity Controlled Oscillations (VCOs) (dendritic inputs or neurons), each with its own frequency depending on speed at a preferred direction. The phase difference of each oscillation in this case expresses the distance travelled by the rat in the oscillation's preferred direction.

According to the model the grid spacing G depends only on the constant β:

$$G = \frac{2}{\sqrt{3}\beta}$$

The average (for all directions) intrinsic firing frequency of a grid cell is predicted to depend on f_o, which is the theta frequency when the rat is stationary, the speed s(t) and the grid spacing G:

$$\left\langle f_i(t) \right\rangle_{\phi(t)} = f_0 + \frac{2(\pi + 1)}{\sqrt{3}\pi G} s(t)$$

Theta frequency depends linearly on the speed according to the equation:

$$f_\theta(s(t)) = f_0 + \left\langle \beta \right\rangle s(t)$$

Three main predictions of the theory in the temporal domain are:

1. The EEG theta frequency increases with the rat speed
2. The intrinsic firing frequency increases with the rat speed
3. The intrinsic firing frequency is slightly faster than the theta frequency and the difference depends on the rat's speed

This theory applied to the place cells faces the problem that a place cell has a single field which does not extend in space. However, predictions about the place cell modulation by the theta frequency at a slightly higher frequency, the inversely proportional relation between the size of the field and the difference in the frequencies and the increase of the intrinsic frequency with increasing speed have been verified for the place cells. [2][4][4][3][1][18] [24][15]

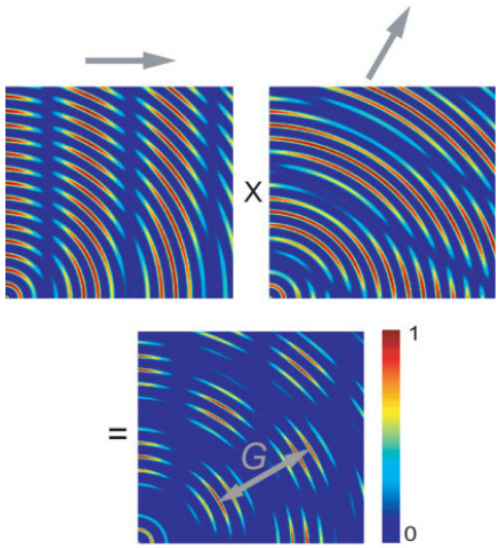

Figure 4-2. Bottom: Interference pattern resulting from two patterns (top) with different preferred directions, as shown by the grey arrows, with an angle of 60^0. The grid pattern is produced by the multiplication of these two. (From [3])

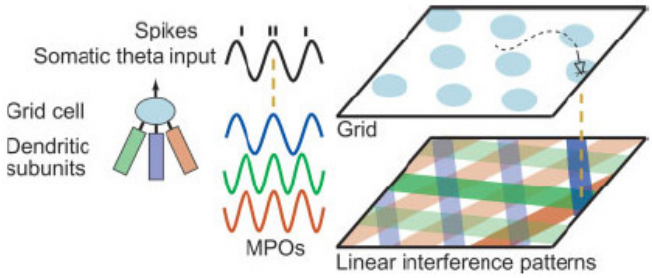

Figure 4-3.Grid cell receiving input from three dendrites: The blue colored MPO when the mouse (shown with the arrow) is moving perpendicular to its preferred direction oscillates at theta frequency while the other two oscillate at higher frequency. Spikes occur at the maximum of the product of the three patterns of each MPO with the theta input. (From [2])

5 Data Analysis

5.1 Data Description and Accessing

The data analyzed in this project were taken from previously conducted experiments with rats in the UCL laboratories. The total number of animals analyzed was 17. Each rat had been tested for a number of trials at specific dates. From the total number of trials for different clusters the analysis was restricted to cells that had already been characterized as grid cells. The duration of the trials has been validated by scanning the data, and for all the analyzed rats it had been 20 minutes.

One or two microdrives, each with four tetrodes, had been implanted above the dorsolateral MEC and advanced so as large amplitude measurements could be taken. Tetrode technology, by simultaneous recording of the spikes at its four electrodes, is able to localize the source neuron in the three-dimensional space of the rat's brain [15]. After the implantation surgery and before the recording started, the animals had been familiarized with the environment for some days. The animals were restricted in a square of a side of 1m and walls of 50cm height, without ceiling. A clearly visible white board placed higher (distal cue) provided directional information. They were able to move freely inside this box and their position was recorded by a camera placed on top of the enclosure. One or two LEDs were placed on the animal's head to make this recording more accurate.

For the recordings of the EEG, the single unit and the position, Axona recording systems (Axona, St Albans, UK) were used. The EEG was recorded in a single channel or in some cases in more, but only the EEG of one channel has been used in the analysis. The sampling frequency for the EEG and for the digitized position measurements have been validated by scanning the data headings for all trials at 250Hz and 50Hz respectively. From the position series the speed and the direction had already been calculated.

These data were stored in the form of Axona files. Previously developed matlab software with a graphical environment (mtint 0.9 – Tint Axona, St Albans, UK) was provided to access and analyze the recorded data. This software is not in its final form and offers the basic tools for data accessing and processing. Apart from some basic screenshots, providing an insight for its functionality, it will not be presented here, since after some usage for inspection of the data, it was decided not to be used for the data analysis. The basic reason for this was that the filter options for the speed provided by the mtint software could not export the intervals for which the speed remains between a certain range of values for a minimum specific duration. The mtint main function (readAxonaData) for reading the data files was used though, while new code had to be written independently to process the data.

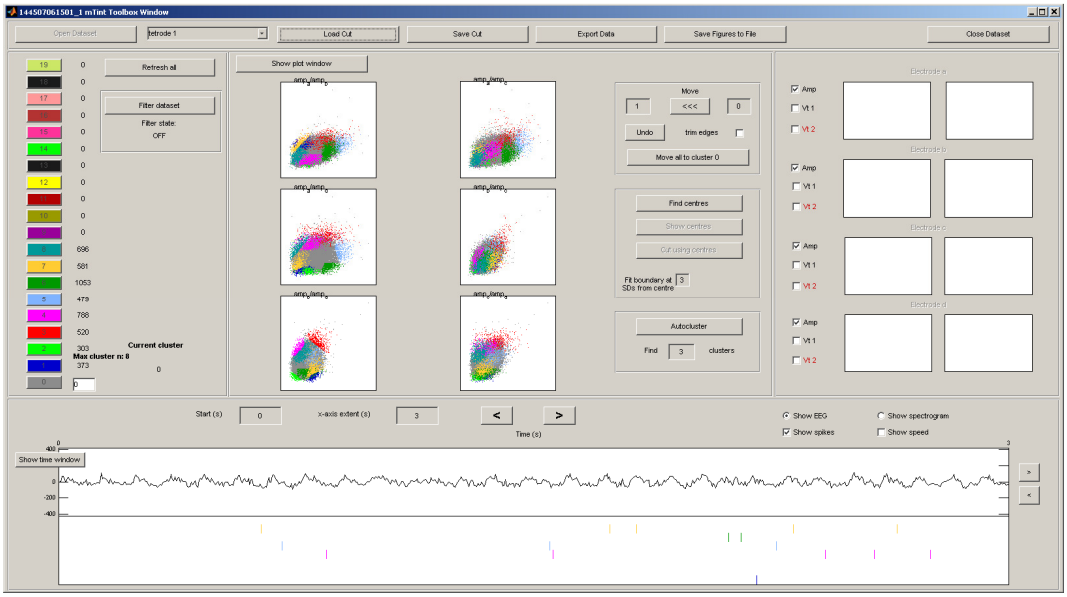

Figure 5-1. Main screen of the Mtint graphical user interface (GUI): On the upper side of the screen buttons for file loading and saving files (e.g. trial files (set files) or clustering data files (cut files)) are located. There is also a dropbox for selecting tetrode. On the left side coloured buttons provide the option for selecting different clusters. In the center of the screen the amplitude vs amplitude plots for the spikes for different tetrode combinations give a visual differentiation for the clusters with tools for clustering. In the lower part the EEG series and the spike trains for selected clusters are presented.

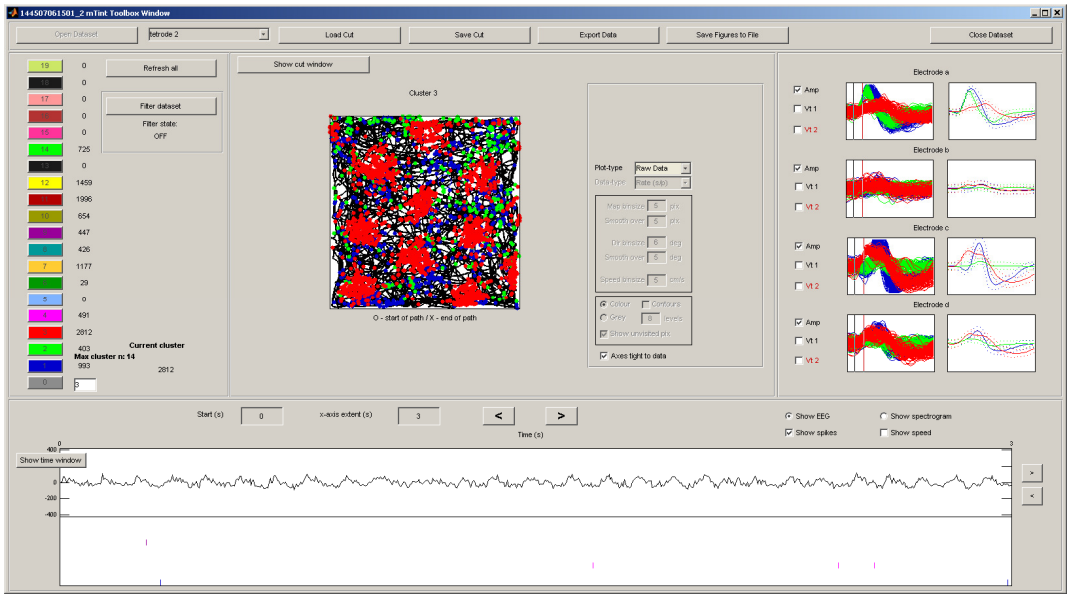

Figure 5-2. Mtint GUI: Map plot showing the trajectory of the rat (black) and the positions of the rat at the corresponding spike times (red) for an identified grid cell. On the right side the electrode spike recordings (waveforms) over time coloured differently for each cluster are presented.

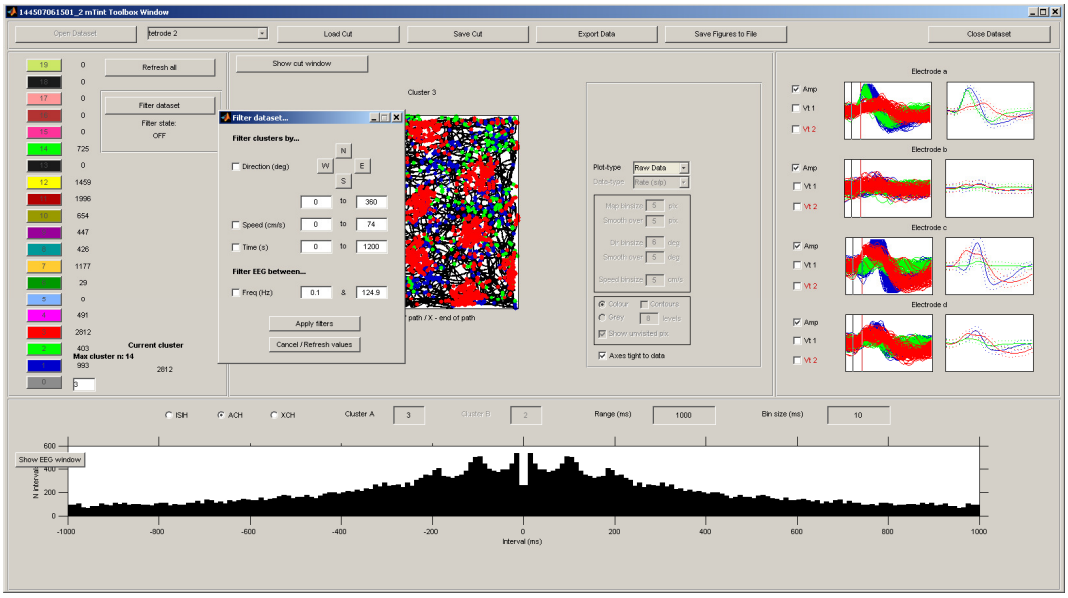

Figure 5-3. Mtint GUI: The filter window for direction, speed, time window and EEG band-pass filtering is activated. In the lower part of the screen options for Inter-Spike-Interval-Histogram (ISIH), Auto-Correlation-Histogram (ACH) (shown) and Cross-Correlation-Histogram for spike trains are provided.

The developed code in its final form can scan selected trial data files starting from a main folder path and automatically performing all the reading and processing. The EEG time-series and the spike trains for specific clusters in different trials were selected and processed in each run, for even multiple speed ranges which were declared in the beginning. The main algorithm was executed first for the following speed intervals:

a) $0<v<5$cm/s and $5<v<50$cm/s

The procedures described later on refer to the first case (a) but they were repeated in the same way for cases (b) and (c):

b) $0<v<10$cm/s and $10<v<50$cm/s
c) $0<v<10$cm/s, $10<v<20$cm/s and $20<v<30$cm/s

The width of the intervals at the third case was chosen so as to allow for an adequate number of intervals with the minimum duration of 0.5s which was kept the same for all cases.

The data analysis methods followed in this essay are for their most part similar to those described in [18] by Jeewajee and colleagues.

The final calculated quantities for each speed interval were:

- total duration
- estimated theta frequency
- SNR for the theta frequency
- total number of spikes
- estimated intrinsic frequency
- SNR for the intrinsic frequency

The total number of clusters given for this study was 140. A number of them though, 34, could not be read successfully by the readAxonaData function because of a high percentage of unreliable position recordings. For an additional one there were no spikes recorded in the corresponding file (cut file). Overall, the total number of analyzed clusters was 115.

The mtint suite provides the tools for characterization of the cells as grid cells and microscopic analysis of brain sections for the position of the tetrode can verify the characterization [18].

5.2 Data Processing

5.2.1 EEG

The EEG timeseries was filtered in order to contain only the intervals ("selected intervals") for which the speed, for a continuous duration of more than 0.5s is less (slow run) than or greater (fast run) than 5cm/s. For each case all the timeseries were tappered near the start and the end (with a half Hanning window of 5 samples width) and concatenated after the mean value for each interval had been subtracted in order to get rid of the constant component. A Fourier transform of 2^{20} elements, for increased resolution, was applied then to acquire the spectral components of the EEG; a band-pass filter of 0.34-125Hz had been applied before the sampling at 250Hz. Therefore, a static frequency content for the EEG had been corresponded to the whole collection of intervals of speed less than 5cm/s and a different one to the whole collection of intervals of speed greater than 5cm/s, resulting as the average power spectrum during these intervals. A different approach had been followed in [18] where, after a relatively narrow band-pass sinc filtering of the range 6-12Hz, an analytic time-dependent signal had been created from a Hilbert transform so as the phase and the instant frequency over time could be supplied. Since, at low speeds, as in our case, the existence of theta oscillation is a question to be answered; such a filtering was not applied, because it would alter significantly the characteristics of the EEG timeseries. In order to determine the theta frequency, the frequency component of the maximum power in the range of 7-14Hz (1 octave) was selected and an estimation of the SNR was calculated by taking the power for an interval of a width $\pm$1Hz centered on the maximum divided by the power for the rest of the frequency components in the range of 7-14Hz. A smoothing on the power spectrum graph had been previously applied with a Gaussian

kernel of approximately 0.25Hz width. Scanning in the range of 4-14Hz was also run with the same results apart from two cases which already had low SNR. An alternative approach for the estimation of the theta frequency and phase had been followed in [13] by determining the zero crossing points and fitting independent sinusoidal waves, but again the level of noise and the unknown characteristics of the EEG timeseries, did not allow such an approach for our case .

5.2.2 Spike Trains

For each identified grid cell the intrinsic firing frequency (f_i) was estimated for both low (<5cm/s) and high (>5cm/s) speed intervals. The corresponding spike trains for each run were selected and spectral analysis was conducted in order to estimate f_i. For each spike train an autocorrelation diagram was computed by equivalently constructing the histogram of the spike distances for all spike pairs (Auto-Correlation Histogram or ACH). The bin used was of 2ms and a maximum time distance of one second was allowed. All the histograms were collected for the slow and fast speed intervals and added separately without weighting since the number of the spikes was alone a weighting factor. After the Fourier transform (2^{15} elements) the frequency of the maximum power was determined in the range of 7-11Hz and the SNR was estimated by taking the power for an interval of a width ±.5Hz centered on the maximum divided by the power for the rest of the frequency components in the range of 7-11Hz.

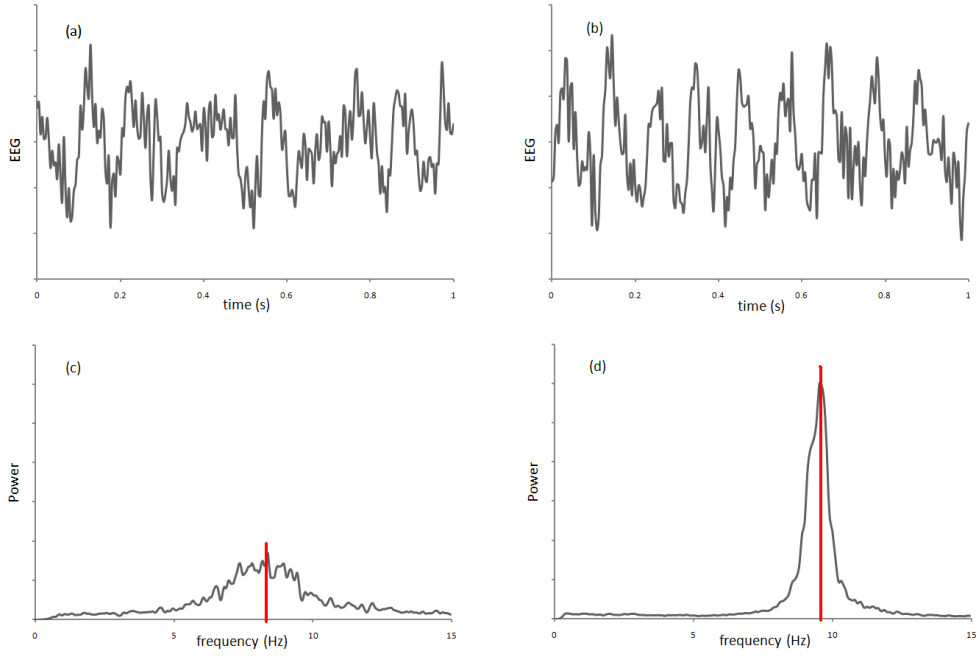

Figure 5-4. Top: EEG timeseries for a duration of 1s of the same trial when (a) v<5cm/s and (b) v>5cm/s. Bottom: Power spectrum for the EEG of the previous trial for v<5cm/s (c) and v>5cm/s (d) with same arbitrary units.

(c): Theta frequency = 8.37Hz and SNR=1.13

(d): Theta frequency = 9.57Hz and SNR=4.38

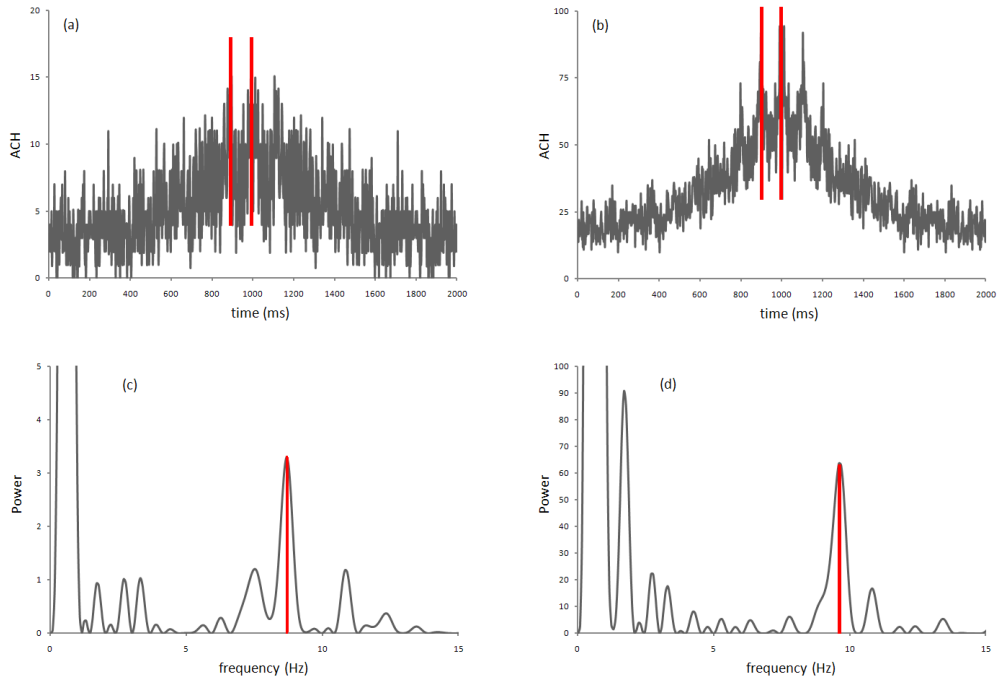

Figure 5-5. Top: Autocorrelograms for spike train when (a) v<5cm/s and (b) v>5cm/s for a grid cell. These autocorrelograms are the result of the summation of the ACHs for each time interval for the slow and fast runs. Bottom: power spectrum in arbitrary units for the previous cases, (c) v<5cm/s and (d) v>5cm/s. The total power for the case of (d) is approximately 5 times that of case (c) because of the higher number of total spikes. From the Fourier transform of the autocorrelograms the intrinsic frequencies and the corresponding SNRs are calculated.

(c): Intrinsic frequency f_i= 8.64Hz and SNR=1.29

(d): Intrinsic frequency f_i= 9.58Hz and SNR=2.42

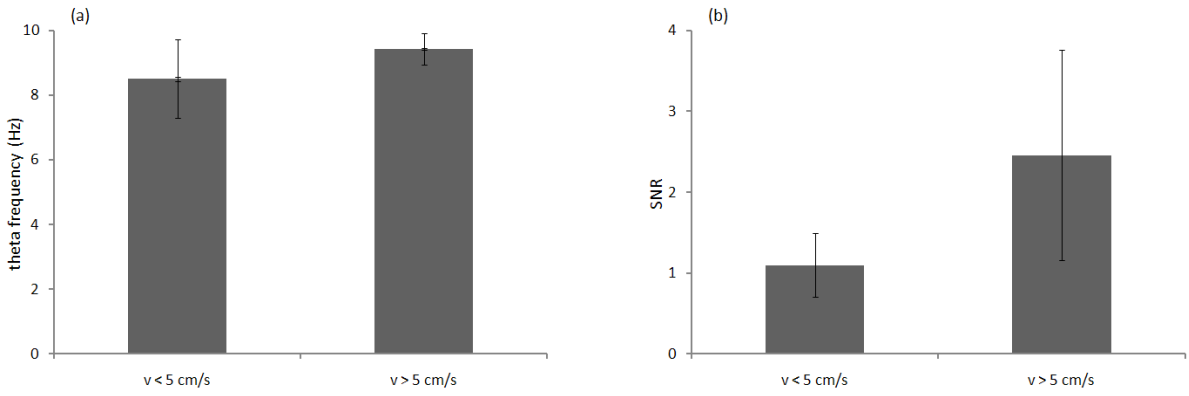

Figure 5-6. Theta frequency (a) and SNR for the theta frequency (b) for all trials. The average is weighted by the intervals duration for v<5cm/s and v>5cm/s for each trial.

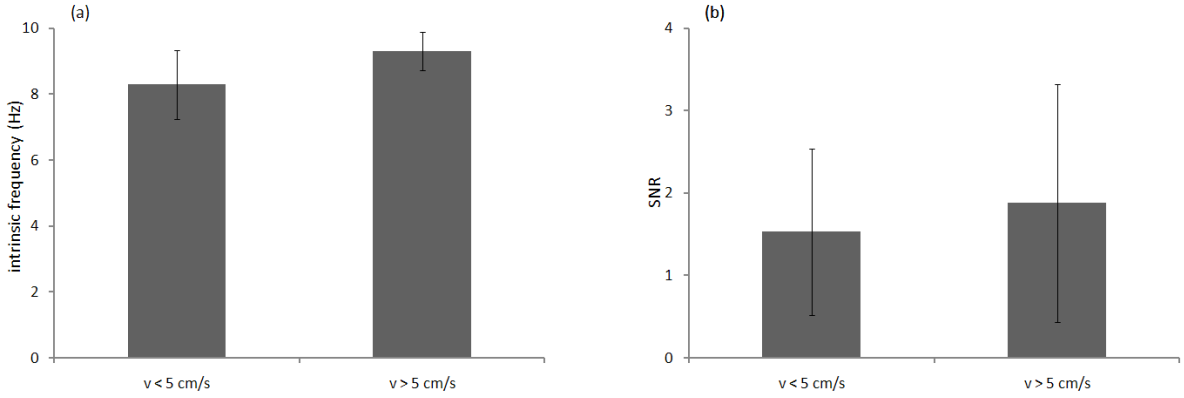

Figure 5-7. Intrinsic firing frequency (a) and SNR for the intrinsic firing frequency (b) for grid cells of all trials. The average is weighted by the number of spikes for v<5cm/s and v>5cm/s for each grid cell in all the trials.

	Theta frequency (Hz)	SNR for theta frequency	Intrinsic frequency (Hz)	SNR for intrinsic frequency
v < 5 cm/s	**8.50**	**1.10**	**8.29**	**1.53**
v > 5 cm/s	**9.42**	**2.46**	**9.32**	**1.88**

Table 5-1. Theta frequency, SNR for the theta frequency, grid cells intrinsic firing frequency and the corresponding SNR averaged for all trials for v<5cm/s and v>5cm/s.

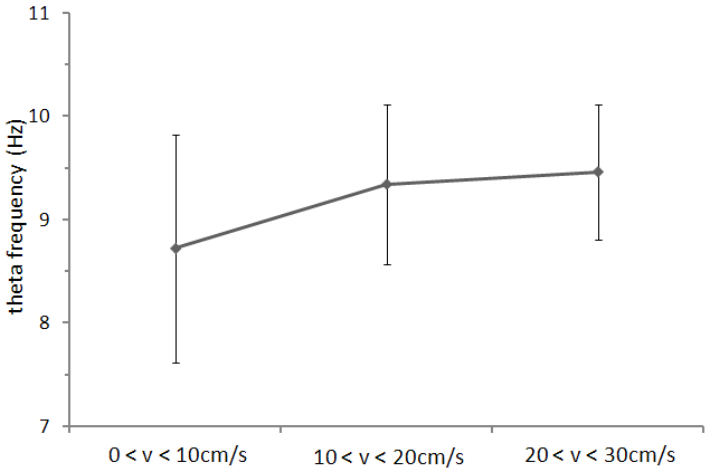

Figure 5-8. Theta frequency dependence on running speed. The theta frequency shown on this diagram is the average of theta frequency for each trial and speed interval weighted by the speed intervals' duration. Linear regression for these data gives y-intercept of 8.62Hz (at zero speed) and a slope of 0.037cm/s/Hz.

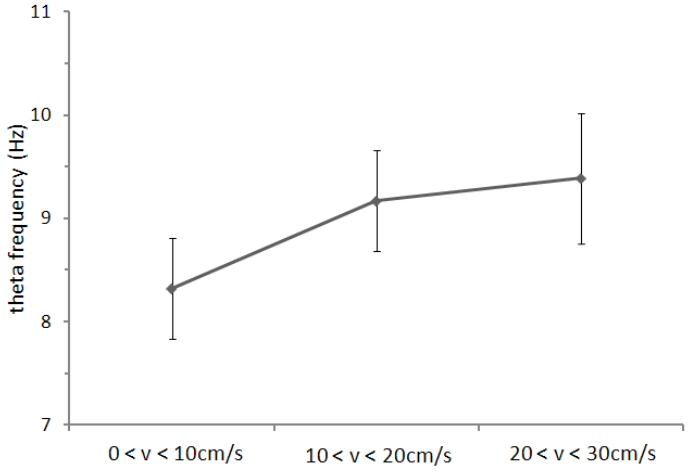

Figure 5-9. Theta frequency dependence on running speed. The theta frequency shown on this diagram is the average of theta frequency for each trial and speed interval weighted by the speed intervals' duration. The trials that have been used in this calculation have been filtered so as not to include values of theta frequency greater than 11Hz and SNR less than 1. Linear regression for these data gives y-intercept of 8.16Hz (at zero speed) and a slope of 0.05cm/s/Hz.

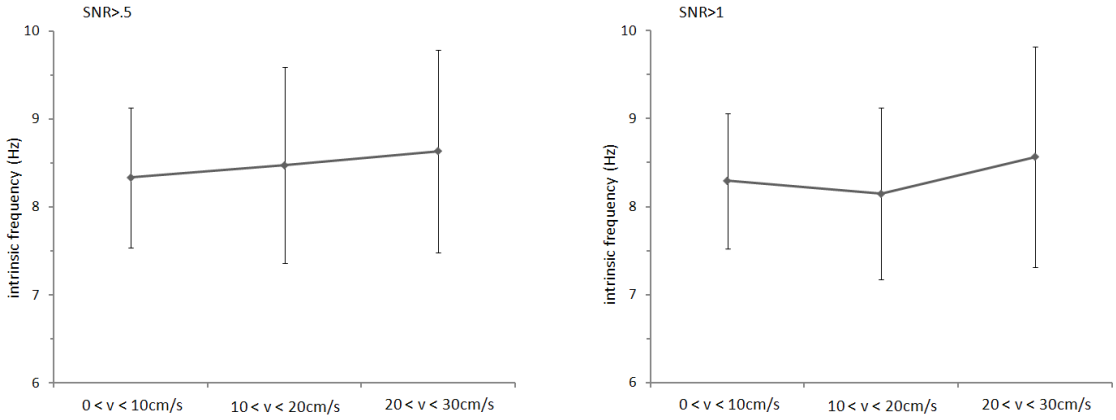

Figure 5-10. Intrinsic firing frequency dependence on running speed for two filtering criteria for the SNR. The frequency depicted is the average of the firing frequency for each cluster and speed interval weighted by the total number of spikes. Linear regression data for both cases are presented on Table 5-2.

Intrinsic firing frequency	**SNR>0.5**	**SNR>1.0**	**Mean value**
y-intercept (Hz)	**8.25**	**8.13**	**8.19±0.08**
Slope (cm/s/Hz)	**0.015**	**0.013**	**0.014±0.001**

Table 5-2. Linear regression for the dependence of intrinsic firing frequency on the running speed based on two calculations for different SNR filtering criteria (SNR>0.5 and SNR>1) with the resulting mean values.

6 Discussion

The theta frequency calculated from the EEG data, as it is expected, has a much lower SNR in the case of low speeds, meaning that the power of the dominating frequency is decreasing when longer periods of no translational movement are recorded for the rat (case when speed is less than 5cm/s) (Figure 5-6). The t-theta pattern is lost in the irregular oscillation of the EEG which is observed as noise. In intervals of higher speed a dominant theta frequency is certain as it is confirmed by the high SNR. It is observed also that the mean theta frequency for speeds less than 5cm/s is lower than the mean theta frequency for speeds larger than 5cm/s. The averaging has been done once for each trial even though in some cases multiple clusters' data of the same trial are included in the data. The weighting factor used was the total duration of the selected speed intervals.

In the case of the intrinsic firing frequency of the grid cells similar arguments hold (Figure 5-7). The SNR is lower in lower speeds, as the theta modulation is not strong, and higher in greater speeds. The value of the frequency is also low at lower speeds and increases in higher speeds. The averaging has been done for all the clusters and the weighting factor was the number of spikes for each time interval.

It is observed that the resulting theta frequency has higher values than the intrinsic firing frequency for all speed intervals. This is normally not expected and is not consistent with the phase precession prediction of the theory. An explanation could be that the range of the frequency scanning in order to locate the maximum is not the same and the results are biased towards a higher theta frequency (scanned in the range of 7-14Hz) and a lower intrinsic frequency (scanned in the range of 7-11Hz).

However, during the processing a lot of different ranges even common for the two frequencies had been scanned and no significant change had occurred. The characteristics of the data are such though, that the theta frequency estimation is quite accurate and robust in a wide range of scanning frequencies while the intrinsic frequency power spectrum has many local maxima rising near the low frequency end which could easily lead to even lower value estimation if the scanning window was extended to the left side. A scanning at 6-12Hz was finally conducted however, as well.

Another explanation could be that the averaging of the theta frequency is done for different trials whereas that of the intrinsic frequency is done for different clusters. Since some trials contain more than one cluster a biased selection of clusters (e.g. more clusters from trials with low theta frequency) could influence the average value. However, averaging of theta frequency keeping multiple trials was also conducted and the results did not change significantly.

What seemed to improve, but not sufficiently, the overestimation of theta frequency was to filter out theta frequencies over 11Hz and all those with SNR<1 as being either not theta oscillations or not reliable enough (Figure 5-9). This resulted in lower values for the theta frequency and linear regression resulted in acceptable value for low speeds but a higher rate of increase in relation to intrinsic frequency leads to the same problem in higher speeds.

In a different approach, by defining as theta modulated cells those for which the SNR for the intrinsic firing frequency f_i is greater than 1 (meaning signal power is greater than that of the total noise in the scanning frequency range), we counted the ones that have f_i greater than the estimated theta, i.e. exhibit phase precession. For both cases, v<5cm/s and v>5cm/s and for different scanning ranges (7-14Hz, 6-12Hz) we concluded to Table 6-1.

Cells that exhibit phase precession	N	Total theta modulated cells	percentage	N	Total theta modulated cells	percentage
	v< 5cm/s			v > 5cm/s		
7-14 (Hz)	25	66	38%	34	85	40%
6-12 (Hz)	13	37	35%	28	68	41%

Table 6-1. Number of theta modulated cells that present phase precession for v<5cm/s and v>5cm/s, for different scanning ranges.

It is observed then, that the total number of cells that exhibit phase precession increases with increasing speed. Furthermore, despite the fact that the number of theta modulated cells increases as well, the percentage of the cells that exhibit phase precession among the theta modulated cells is larger in higher speeds.

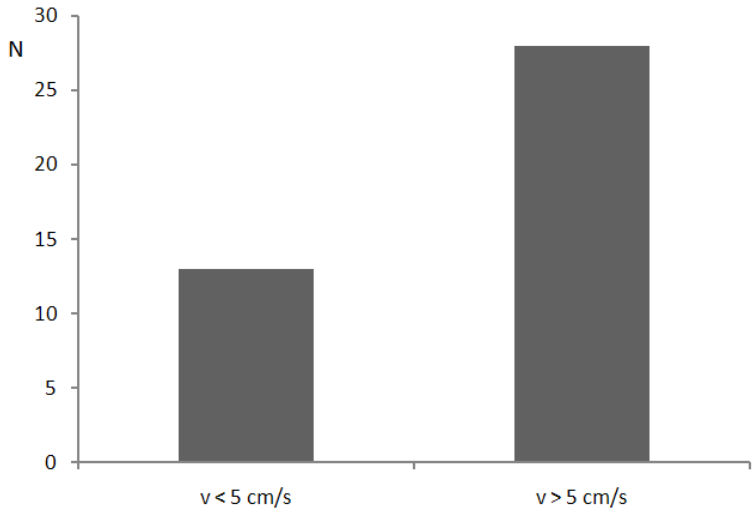

Figure 6-1. Total number of theta modulated cells exhibiting phase precession for the cases of v<5cm/s and v>5cm/s (the frequencies, theta and intrinsic, and the respective SNRs have been calculated in the range of 6-12Hz).

7 Conclusions

Overall, the main temporal predictions of the oscillatory interference theory regarding the increase of both the theta frequency and the intrinsic firing frequency with the increase of the rat speed were validated. A probable overestimation of the theta frequency or underestimation of the intrinsic frequency did not allow at speeds lower than 5cm/s, but unfortunately also at speeds greater than 5cm/s, to validate the phase precession prediction of the theory. However, a different approach led to the conclusion that the number of the grid cells that exhibit phase precession increases with the increase of speed. A possible improvement in the quality of data could be an option of choosing for each interval the channel for which the timeseries of the EEG presented the best SNR.

8 Acknowledgements

I would like to thank my two supervisors, John O' Keefe and Neil Burgess, as well as Ali Jeewajee for their help, guidance and support during this project. My studying at UCL CoMPLEX is possible because of my scholarship by the Greek State Scholarship Foundation (IKY). CoMPLEX is an EPSRC funded Doctoral Training Centre.

9 References

[1] J. O'Keefe and N. Burgess, "Dual phase and rate coding in hippocampal place cells: theoretical significance and relationship to entorhinal grid cells," *Hippocampus*, vol. 15, no. 7, pp. 853-866, 2005.

[2] N. Burgess, C. Barry, and J. O'Keefe, "An oscillatory interference model of grid cell firing," *Hippocampus*, vol. 17, no. 9, pp. 801-812, 2007.

[3] N. Burgess, "Grid cells and theta as oscillatory interference: theory and predictions," *Hippocampus*, vol. 18, no. 12, pp. 1157-1174, 2008.

[4] E. I. Moser, E. Kropff, and M.-B. Moser, "Place Cells, Grid Cells, and the Brain's Spatial Representation System," *Annual Review of Neuroscience*, vol. 31, no. 1, pp. 69-89, Jul. 2008.

[5] P. Andersen, R. Morris, T. Bliss, and J. O'Keefe, Eds., *The hippocampus book*. Oxford□ ;;New York: Oxford University Press, 2007.

[6] P. Andersen, R. Morris, D. Amaral, T. Bliss, and J. O'Keefe, "Historical Perspective: Proposed Functions, Biological Characteristics, and Neurobiological Models of the Hippocampus," in *The hippocampus book*, P. Andersen, R. Morris, D. Amaral, T. Bliss, and J. O'Keefe, Eds. Oxford□ ;New York: Oxford University Press, 2007, pp. 9-36.

[7] D. Amaral and P. Lavenex, "Hippocampal Neuroanatomy," in *The hippocampus book*, P. Andersen, R. Morris, D. Amaral, T. Bliss, and J. O'Keefe, Eds. Oxford□ ;New York: Oxford University Press, 2007, pp. 37-114.

[8] C. H. Vanderwolf, "Hippocampal electrical activity and voluntary movement in the rat," *Electroencephalography and Clinical Neurophysiology*, vol. 26, no. 4, pp. 407-418, Apr. 1969.

[9] U. Slawinska and S. Kasicki, "The frequency of rat's hippocampal theta rhythm is related to the speed of locomotion," *Brain Research*, vol. 796, no. 1-2, pp. 327-331, Jun. 1998.

[10] J. O'Keefe, "Hippocampal Neurophysiology in the Behaving Animal," in *The hippocampus book*, P. Andersen, R. Morris, D. Amaral, T. Bliss, and J. O'Keefe, Eds. Oxford□ ;New York: Oxford University Press, 2007, pp. 475-548.

[11] J. O'Keefe and J. Dostrovsky, "The hippocampus as a spatial map. Preliminary evidence from unit activity in the freely-moving rat," *Brain Research*, vol. 34, no. 1, pp. 171-175, Nov. 1971.

[12] J. O'Keefe, "Place units in the hippocampus of the freely moving rat," *Experimental Neurology*, vol. 51, no. 1, pp. 78-109, 1976.

[13] J. O'Keefe and M. L. Recce, "Phase relationship between hippocampal place units and the EEG theta rhythm," *Hippocampus*, vol. 3, no. 3, pp. 317-330, Jul. 1993.

[14] W. E. Skaggs, B. L. McNaughton, M. A. Wilson, and C. A. Barnes, "Theta phase precession in hippocampal neuronal populations and the compression of temporal sequences," *Hippocampus*, vol. 6, no. 2, pp. 149-172, 1996.

[15] N. Burgess, M. Recce, and J. O'Keefe, "A model of hippocampal function," *Neural Networks*, vol. 7, no. 6-7, pp. 1065-1081, 1994.

[16] M. Fyhn, S. Molden, M. P. Witter, E. I. Moser, and M.-B. Moser, "Spatial Representation in the Entorhinal Cortex," *Science*, vol. 305, no. 5688, pp. 1258 -1264, 2004.

[17] T. Hafting, M. Fyhn, S. Molden, M.-B. Moser, and E. I. Moser, "Microstructure of a spatial map in the entorhinal cortex," *Nature*, vol. 436, no. 7052, pp. 801-806, Jun. 2005.

[18] A. Jeewajee, C. Barry, J. O'Keefe, and N. Burgess, "Grid cells and theta as oscillatory interference: electrophysiological data from freely moving rats," *Hippocampus*, vol. 18, no. 12, pp. 1175-1185, 2008.
[19] T. Hafting, M. Fyhn, T. Bonnevie, M.-B. Moser, and E. I. Moser, "Hippocampus-independent phase precession in entorhinal grid cells," *Nature*, vol. 453, no. 7199, pp. 1248-1252, May. 2008.
[20] F. Sargolini, "Conjunctive Representation of Position, Direction, and Velocity in Entorhinal Cortex," *Science*, vol. 312, no. 5774, pp. 758-762, May. 2006.
[21] M. Fyhn, T. Hafting, A. Treves, M.-B. Moser, and E. I. Moser, "Hippocampal remapping and grid realignment in entorhinal cortex," *Nature*, vol. 446, no. 7132, pp. 190-194, Mar. 2007.
[22] C. Barry, R. Hayman, N. Burgess, and K. J. Jeffery, "Experience-dependent rescaling of entorhinal grids," *Nature Neuroscience*, vol. 10, no. 6, pp. 682-684, Jun. 2007.
[23] M. C. Fuhs and D. S. Touretzky, "A Spin Glass Model of Path Integration in Rat Medial Entorhinal Cortex," *The Journal of Neuroscience*, vol. 26, no. 16, pp. 4266 -4276, Apr. 2006.
[24] C. Geisler, D. Robbe, M. Zugaro, A. Sirota, and G. Buzsáki, "Hippocampal place cell assemblies are speed-controlled oscillators," *Proceedings of the National Academy of Sciences*, vol. 104, no. 19, pp. 8149 -8154, May. 2007.